1-25-2012

Rovibrationally Resolved Direct Photodissociation through the Lyman and Werner Transitions of H_2 for FUV/X-Ray-Irradiated Environments

C. D. Gay
University of Georgia

N. P. Abel
University of Cincinnati

R. L. Porter
University of Georgia

P. C. Stancil
University of Georgia

Gary J. Ferland
University of Kentucky, gary@uky.edu

See next page for additional authors

Rovibrationally Resolved Direct Photodissociation through the Lyman and Werner Transitions of H_2 for FUV/X-Ray-Irradiated Environments

Digital Object Identifier (DOI)
https://doi.org/10.1088/0004-637X/746/1/78

Notes/Citation Information
Published in *The Astrophysical Journal*, v. 746, no. 1, 78, p. 1-8.

Authors
C. D. Gay, N. P. Abel, R. L. Porter, P. C. Stancil, Gary J. Ferland, G. Shaw, P. A. M. vanHoof, and R. J. R. Williams

The Astrophysical Journal, 746:78 (8pp), 2012 February 10 doi:10.1088/0004-637X/746/1/78

ROVIBRATIONALLY RESOLVED DIRECT PHOTODISSOCIATION THROUGH THE LYMAN AND WERNER TRANSITIONS OF H_2 FOR FUV/X-RAY-IRRADIATED ENVIRONMENTS

C. D. Gay[1], N. P. Abel[2], R. L. Porter[1], P. C. Stancil[1], G. J. Ferland[3], G. Shaw[4], P. A. M. van Hoof[5], and R. J. R. Williams[6]
[1] Department of Physics and Astronomy and Center for Simulational Physics, The University of Georgia, Athens, GA 30602-2451, USA; cgay1383@gmail.com, ryanlporter@gmail.com, stancil@physast.uga.edu
[2] Math, Computers, Geology, and Physics Department, University of Cincinnati, Clermont Campus, Batavia, OH 45103, USA; npabel2@gmail.com
[3] Department of Physics and Astronomy, University of Kentucky, Lexington, KY, USA; gary@pa.uky.edu
[4] Centre for Excellence in Basic Sciences, UM-DAE, Vidhyanagari Campus, Mumbai-400098, India; gargishaw@gmail.com
[5] Royal Observatory of Belgium, Ringlaan 3, 1180 Brussels, Belgium; p.vanhoof@oma.be
[6] AWE plc, Aldermaston, Reading RG7 4PR, UK; robin.williams@awe.co.uk
Received 2011 March 10; accepted 2011 November 23; published 2012 January 25

ABSTRACT

Using ab initio potential curves and dipole transition moments, cross-section calculations were performed for the direct continuum photodissociation of H_2 through the $B^1\Sigma_u^+ \leftarrow X^1\Sigma_g^+$ (Lyman) and $C^1\Pi_u \leftarrow X^1\Sigma_g^+$ (Werner) transitions. Partial cross-sections were obtained for wavelengths from 100 Å to the dissociation threshold between the upper electronic state and each of the 301 bound rovibrational levels $v''J''$ within the ground electronic state. The resulting cross-sections are incorporated into three representative classes of interstellar gas models: diffuse clouds, photon-dominated regions, and X-ray-dominated regions (XDRs). The models, which used the CLOUDY plasma/molecular spectra simulation code, demonstrate that direct photodissociation is comparable to fluorescent dissociation (or spontaneous radiative dissociation, the Solomon process) as an H_2 destruction mechanism in intense far-ultraviolet or X-ray-irradiated gas. In particular, changes in H_2 rotational column densities are found to be as large as 20% in the XDR model with the inclusion of direct photodissociation. The photodestruction rate from some high-lying rovibrational levels can be enhanced by pumping from H Lyβ due to a wavelength coincidence with cross-section resonances resulting from quasi-bound levels of the upper electronic states. Given the relatively large size of the photodissociation data set, a strategy is described to create truncated, but reliable, cross-section data consistent with the wavelength resolving power of typical observations.

Key words: ISM: molecules – molecular data – molecular processes – photon-dominated region (PDR) – X-rays: ISM

Online-only material: color figures

1. INTRODUCTION

While H_2 is primarily created on grains in the interstellar medium (ISM), a variety of processes contribute to its destruction depending on the local conditions of the environment. The Solomon process, i.e., bound–bound resonant absorption through the Lyman and Werner bands followed by fluorescent decay into the ground state continuum,

$$H_2(X, v''J'') + h\nu \rightarrow H_2^*(B, C; v'J') \rightarrow H(1s) + H(1s) + h\nu', \quad (1)$$

is generally believed to be the dominant H_2 destruction path until self-shielding at large column densities sets in (Stecher & Williams 1967; Federman et al. 1979; Abgrall et al. 1992, 2000). However, for moderate column densities, the direct continuum photodissociation process,

$$H_2(X, v''J'') + h\nu \rightarrow H(1s) + H(2p), \quad (2)$$

where photon energies greater than Lyα can remove rovibrationally excited molecular hydrogen, can contribute to the total destruction rate as pointed out by Shull (1978). Most models of UV-irradiated environments exclude this process. An exception was Shull (1978), who utilized the v''-resolved cross-sections for process (2) of Allison & Dalgarno (1969) in his study of UV-pumped H_2 rovibrational lines in dense molecular clouds irradiated by O stars. Recently, the spectral simulation code CLOUDY was updated to include a full microphysical model of H_2 including direct photodissociation of H_2 (Shaw et al. 2005). However, there has been a lack of cross-sections resolved at the J'' rotational level which hinders detailed modeling of H_2 in strongly irradiated environments.

In the present work, we address this issue by computing rovibrationally resolved direct photodissociation cross-sections through the Lyman and Werner continuum of H_2 for all 301 bound rovibrational levels ($v''J''$) in the ground electronic state. The new cross-sections are used in photoionized gas models which demonstrate the importance of continuum photodissociation of H_2 in intense far-ultraviolet (FUV) and X-ray-irradiated environments. Atomic units are used throughout, except where indicated.

2. THEORY OF PHOTODISSOCIATION

2.1. Potential Energies and Dipole Transition Moments

Potential energy data for the $X^1\Sigma^+$ (Wolniewicz 1993, 1995), $B^1\Sigma^+$ (Kolos & Wolniewicz 1968), and $C^1\Pi$ (Kolos & Wolniewicz 1965) electronic states as well as the dipole transition moments between them (Dressler & Wolniewicz 1985) were used in the present study. The ab initio potential energies are available over a range of internuclear distances from $R = 0.1$ to $100.0a_0$, $R = 1.0$ to $14.0a_0$, and $R = 1.0$ to $12.0a_0$ for the X, B, and C states, respectively, while the dipole transition moments are both available over the range $R = 1.0$ to $12.0a_0$.

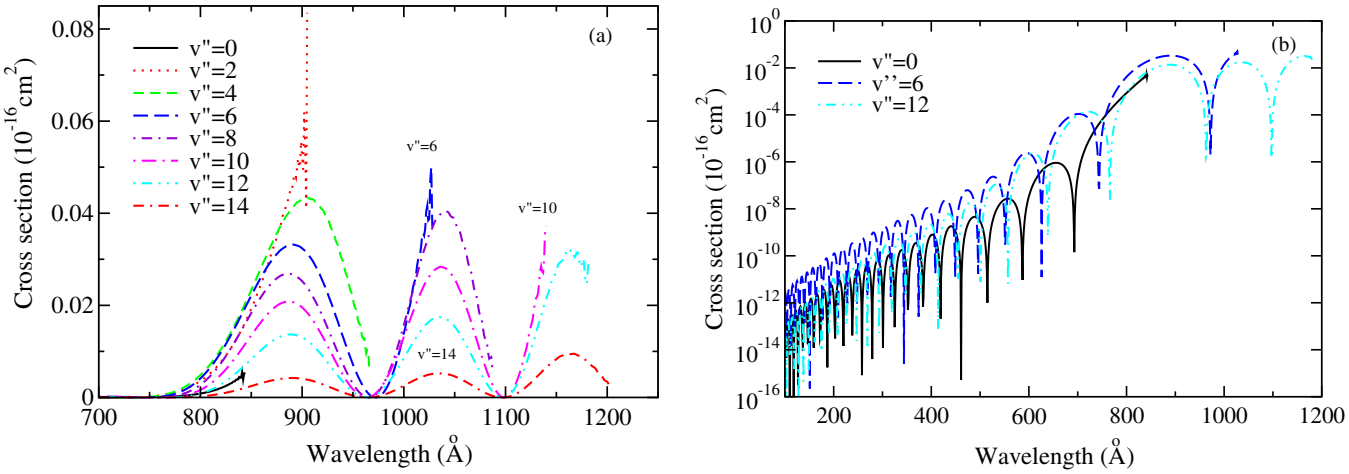

Figure 1. Partial photodissociation cross-sections $\sigma_{v''J''}$ as a function of wavelength for the H_2 $B \leftarrow X$ transition from several vibrational levels v'' and rotational level $J'' = 0$ of the ground electronic state. (a) Linear scale. (b) Logarithmic scale.

(A color version of this figure is available in the online journal.)

To force agreement with the dissociation energy obtained experimentally, the ab initio X ground state potential was smoothly fit to the long-range interaction potential

$$V_X(R) = -\frac{C_6}{R^6} - \frac{C_8}{R^8} - \frac{C_{10}}{R^{10}} - \frac{C_{11}}{R^{11}} - \frac{C_{12}}{R^{12}}, \quad (3)$$

for internuclear distances $R > 100.0a_0$. Dispersion coefficients C_6, C_8, and C_{10} are adopted from Yan et al. (1996), while C_{11} and C_{12} were taken from Bukta & Meath (1974). Similarly, for the B and C states, and for internuclear distances $R > 14.0a_0$ and $R > 12.0a_0$, respectively, the ab initio potentials have been smoothly fit to

$$V_\Lambda(R) = -\frac{C_3}{R^3} - \frac{C_6}{R^6} - \frac{C_8}{R^8}. \quad (4)$$

Here, Λ (the projection of the electronic angular momentum on the internuclear axis) labels the electronic state and the dispersion coefficients, C_3, C_6, and C_8, are taken from Stephens & Dalgarno (1974). At smaller internuclear distances, the ab initio potential curves have been fit to an interaction potential of the form

$$V_\Lambda(R) = a\exp(-bR) + c \quad (5)$$

for $R < 0.1a_0$ for the X state and for $R < 1.0a_0$ for the B and C states.

For the dipole transition moments $D(R)$, a similar exponential form was fit for both long- and short-range behavior for internuclear distances of $R > 12.0a_0$ and $R < 1.0a_0$, respectively. The dipole transition moments were forced to 0.4208 a.u. at $R = 0$, to bring them into agreement with the united-atom limit value given by Dressler & Wolniewicz (1985).

2.2. Photodissociation Cross Sections

For absorption into the rovibrational continuum of electronic state f from the rovibrational level $v''J''$ of electronic state i, the partial rotational photodissociation cross-section is given by (e.g., Kirby & van Dishoeck 1988; Weck et al. 2003)

$$\sigma_{v''J''} = 2.69 \times 10^{-18}\Delta E_{k'J',v''J''}\frac{1}{2J''+1} \times \sum_{J'=J''-1}^{J''+1} S_{J'J''}|D^{fi}_{k'J',v''J''}|^2 \text{ cm}^2, \quad (6)$$

where $\Delta E_{k'J',v''J''}$ is the energy of the absorbed photon and $S_{J'J''}$ are the Hönl–London factors defined for the $B^1\Sigma_u^+ \leftarrow X^1\Sigma_g^+$ transition as

$$S_{J'J''} = \begin{cases} J'', & J' = J'' - 1 \text{ (P branch)} \\ J''+1, & J' = J''+1 \text{ (R branch)} \end{cases} \quad (7)$$

and for the $C^1\Pi_u \leftarrow X^1\Sigma_g^+$ transition as

$$S_{J'J''} = \begin{cases} (J''-1)/2, & J' = J''-1 \text{ (P branch)} \\ (2J''+1)/2, & J' = J'' \text{ (Q branch)} \\ (J''+2)/2, & J' = J''+1 \text{ (R branch)}, \end{cases} \quad (8)$$

according to the convention given by Whiting & Nicholls (1974). In Equation (6), the term $D^{fi}_{k'J',v''J''} = \langle\chi_{k'J'}|D^{fi}(R)|\chi_{v''J''}\rangle$ is the matrix element of the electric dipole transition moment for absorption from the state i into the f electronic state. The continuum wave functions $\chi_{k'J'}(R)$ are normalized asymptotically as

$$\chi_{k'J'}(R) \sim \sin\left(k'R - \tfrac{\pi}{2}J' + \delta_{J'}\right), \quad (9)$$

where $\delta_{J'}$ is the phase shift.

Continuum wave functions $\chi_{k'J'}$ were obtained for the B and C states and bound wave functions $\chi_{v''J''}$ were obtained for the X state by solution of the radial Schrödinger equation using a standard numerical method (Cooley 1961). Wave functions were obtained over the internuclear distance range $0.1a_0 \leqslant R \leqslant 200a_0$ on a grid with a stepsize of $1 \times 10^{-3}a_0$.

3. RESULTS AND DISCUSSION

3.1. Photodissociation Cross-sections

Representative partial cross-sections $\sigma_{v''J''}$ for the $B^1\Sigma_u^+ \leftarrow X^1\Sigma_g^+$ and $C^1\Pi_u \leftarrow X^1\Sigma_g^+$ transitions are presented in Figures 1–3.[7,8] Figures 1 and 2 present partial cross-sections $\sigma_{v''J''}$ as a function of wavelength for several vibrational levels

[7] Complete data for the $B \leftarrow X$ and $C \leftarrow X$ photodissociation cross-sections are available online at the UGA Molecular Opacity Project database Web site, http://www.physast.uga.edu/ugamop/.

[8] We note that the $E, F^1\Sigma_g^+ \leftarrow X^1\Sigma_g^+$ transition, where the upper state correlates asymptotically to H(1s)+H(2s), is forbidden.

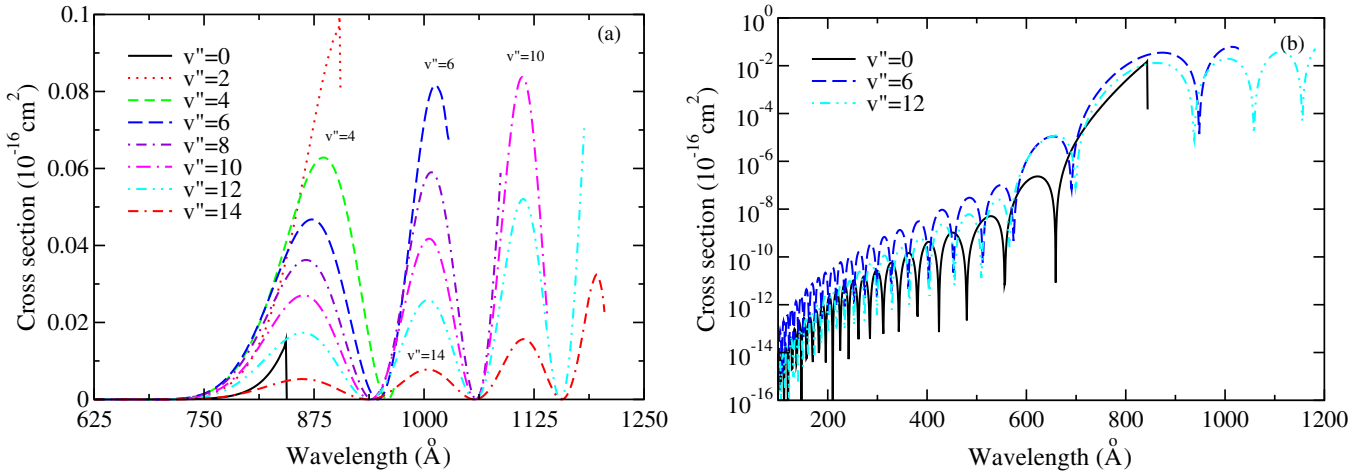

Figure 2. Partial photodissociation cross-sections $\sigma_{v''J''}$ as a function of wavelength for the H_2 $C \leftarrow X$ transition from several vibrational levels v'' and rotational number $J'' = 0$ of the ground electronic state. (a) Linear scale. (b) Logarithmic scale.

(A color version of this figure is available in the online journal.)

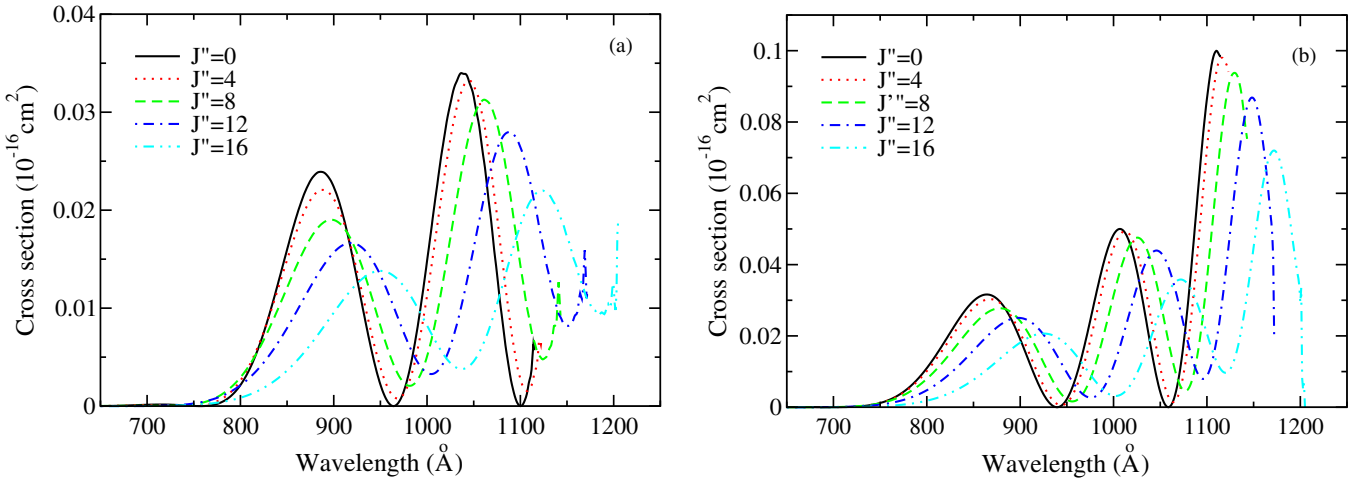

Figure 3. Partial H_2 photodissociation cross-sections $\sigma_{v''J''}$ as a function of wavelength for both transitions from vibrational level $v'' = 9$ and several rotational levels J'' of the ground electronic state. (a) $B \leftarrow X$. (b) $C \leftarrow X$.

(A color version of this figure is available in the online journal.)

v'' of the $X^1\Sigma_g^+$ ground electronic state, all with rotational level $J'' = 0$, for the Lyman and Werner transitions, respectively. These partial cross-sections reveal several nodes and antinodes which are independent of the electronic ground state vibrational number v'' and display quasi-periodic behavior. This is due to the oscillatory character of the continuum wave functions $\chi_{k'J'}$ of the upper states.

Figure 3 displays partial cross-sections as a function of wavelength, but for constant vibrational level $v'' = 9$ in order to explore the differences in the cross-sections over a range of rotational levels J''. We see nodes and antinodes as before, but here increasing values of J'' cause their wavelengths to shift toward higher values. This is because for a particular vibrational level v'', as the rotational level J'' increases, the ground state wave function becomes increasingly dissimilar and the wave function samples a higher and wider part of the ground state electronic potential.

For all calculated partial cross-sections, as displayed in Figures 1–3, the values of the thresholds increase as the rovibrational level $v''J''$ increases, as expected. Further, as a fine photon energy grid was adopted, resonances due to quasi-bound levels in the final electronic states are evident near the thresholds. Earlier calculations of the partial cross-sections for these transitions were performed by Allison & Dalgarno (1969) over all vibrational levels v''; however, they only considered rotational levels $J'' = 0$. Figure 4 demonstrates that our current calculated cross-sections are in reasonable agreement with the earlier results. The small discrepancies are likely due to improvements in the transition dipole moments, long-range potentials, and numerical convergence of the rovibrational wave functions.

3.2. Direct H_2 Photodissociation in FUV/X-Ray-irradiated Gas Models

Direct photodissociation of H_2 has typically been neglected in astrochemical models since the threshold for photodissociation of the ground rovibrational level of $X^1\Sigma_g^+$ is 844 Å, significantly below the Lyman limit (see Figure 5). While the standard UV interstellar radiation field has few photons beyond the Lyman limit, the photodissociation threshold for many rotationally and/or vibrationally excited levels of H_2 occur at longer wavelengths and have significant cross section magnitudes. Such levels can be populated far above their thermal values by, for

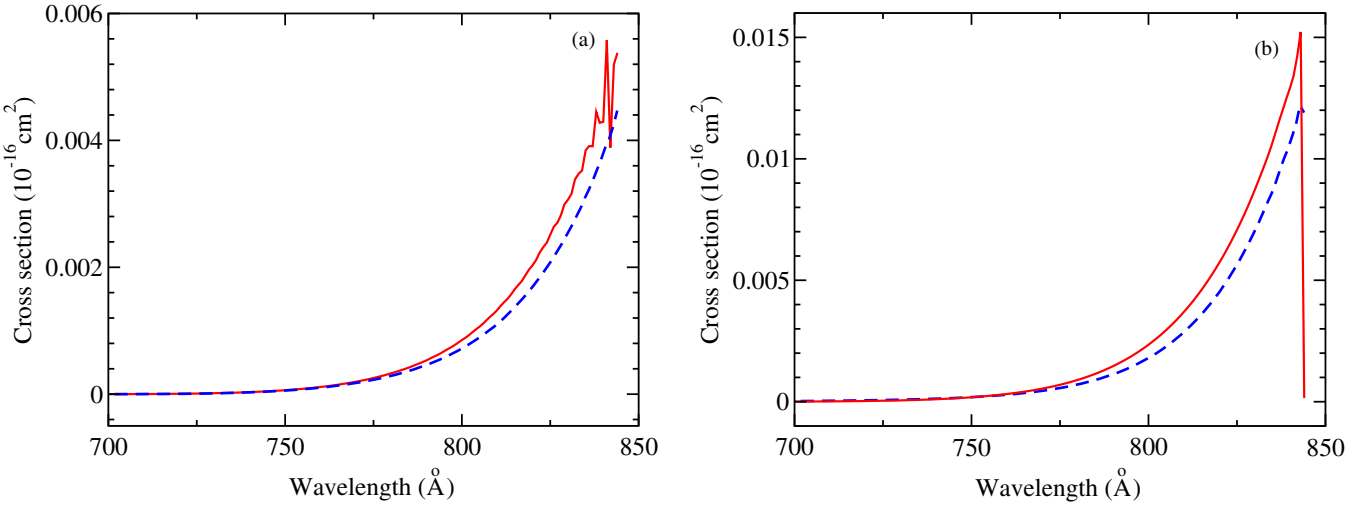

Figure 4. Comparison of partial H_2 photodissociation cross-sections $\sigma_{v''J''}$ as a function of wavelength for transitions from $v'' = 0$, $J'' = 0$ of the ground electronic state. (a) $B \leftarrow X$. (b) $C \leftarrow X$. Dashed line: Allison & Dalgarno (1969). Solid line: current calculation.
(A color version of this figure is available in the online journal.)

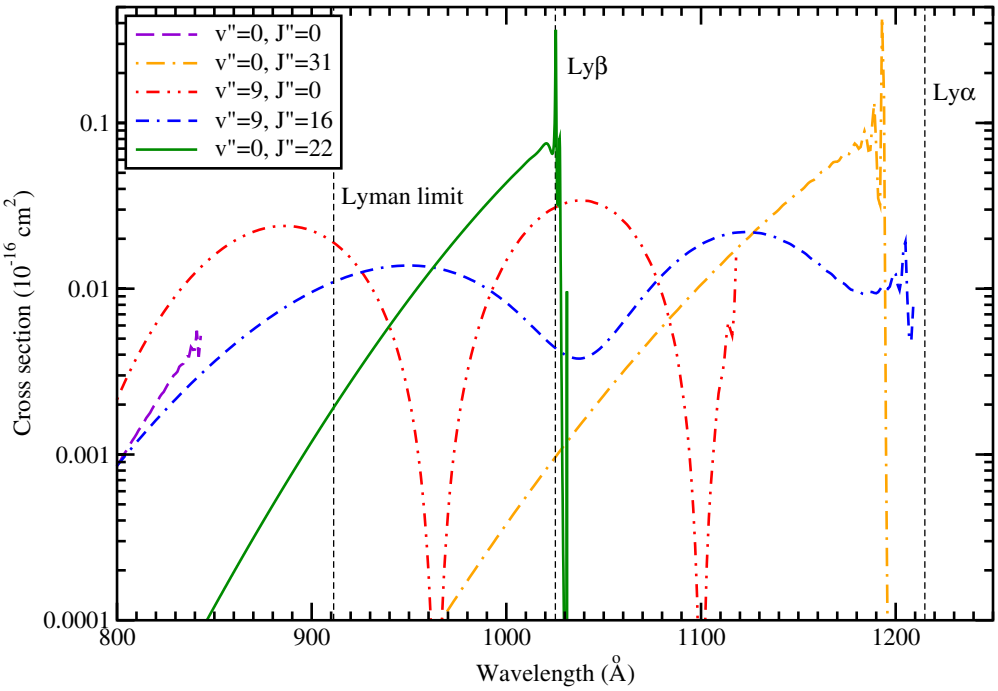

Figure 5. Resonant features in example H_2 $B \leftarrow X$ photodissociation transitions compared to H Lyman features.
(A color version of this figure is available in the online journal.)

example, UV fluorescent processes through bound–bound H_2 Lyman and Werner bands. Therefore, direct photodissociation of H_2 is likely to be an important destruction mechanism in a variety of environments including photon-dominated regions (PDRs; e.g., Bertoldi & Draine 1996) and X-ray-dominated regions (XDRs; e.g., Tiné et al. 1997), and other irradiated scenarios such as gamma-ray bursts through molecular clouds (Draine 2000) and UV radiative feedback in Population III star formation (e.g., Haiman et al. 1996; Miyake et al. 2010). Using the vibrationally resolved cross-sections of Allison & Dalgarno (1969), Coppola et al. (2011) computed H_2 photodissociation rates for a blackbody radiation field and assuming a Boltzmann distribution of vibrational levels for temperatures between 1000 and 50,000 K. They applied their results to the chemistry of the recombination era of the early universe. However, the process is not significant since the cosmic background radiation field has few UV photons at the epoch of H_2 formation (redshift $z < 1000$).

To elucidate the possible importance of H_2 photodissociation in other UV-irradiated environments, we performed several simulations under various conditions. The simulations used a prerelease of the upcoming C10 version of the spectral synthesis code CLOUDY, last described by Ferland et al. (1998), which incorporates the major ionization processes that affect the ionization structure. These include direct photoionization; charge transfer; Auger effects; and dielectronic, collisional, and cosmic-ray ionization. Abel et al. (2005) and Shaw et al. (2005) described advances in its treatment of

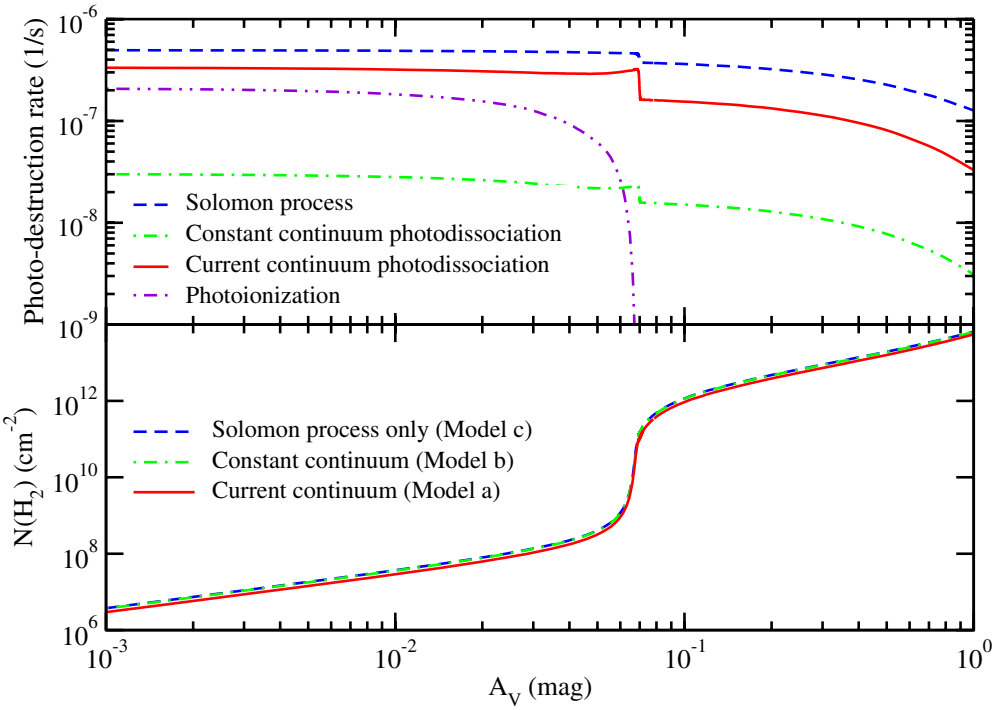

Figure 6. H_2 photodestruction rates (s^{-1}) and $N(H_2)$ (cm^{-2}) for the Orion Veil (Model I) as a function of visual extinction A_V.
(A color version of this figure is available in the online journal.)

molecular processes, while van Hoof et al. (2004) described the grain physics.

We considered three separate scenarios, each based on models described elsewhere. Therefore, we only describe the essential details here, and point the reader to the other works for a complete description of each simulation. The three models (which are all part of the CLOUDY test suite) are as follows.

I. The Orion Veil model from Abel et al. (2004, 2006), which computes the physical conditions in the foreground cloud along the line of sight toward the ionizing stars of the Orion Nebula, and physically associated with Orion. This environment is an example of a high UV ($G_0 \sim 10^4$–10^5) pumped diffuse cloud where, due to the high UV flux, large grains, and low extinction ($A_V \sim 1.6$), the total H_2 column density is $\sim 10^{15}$ cm^{-2}, with most of the H_2 abundance residing in states with $J'' > 2$.

II. The Leiden F2 model from Röllig et al. (2007), which is an example of a typical PDR ($G_0 = 10^5$), where at the innermost molecular region almost all of the hydrogen and carbon atoms have been converted to H_2 and CO, respectively.

III. An XDR model of gas irradiated by an active galactic nucleus (AGN) continuum, which is based on the models computed by Abel et al. (2009) of AGNs and starbursts where the H^+ region and molecular region are in pressure equilibrium. The penetration of X-rays deep into the molecular region can lead to a significant amount of radiation with photon energies greater than 13.6 eV (the Lyman limit) in regions where H_2 is abundant. The AGN spectrum therefore produces radiation which leads to direct H_2 dissociation beyond the H^+ ionization front, thereby affecting the emission spectrum. An XDR can have molecular, density, and thermal structures which differ significantly from a typical PDR (Meijerink & Spaans 2005).

Note that G_0 is the intensity of the radiation field in Habing units where $G_0 = 1$ corresponds to the standard ISM field.

These three models represent a broad range of conditions. For each, we computed the H_2 density structure and emission-line spectrum for three different considerations of the direct H_2 photodissociation rate which include (a) the rovibrationally resolved photodissociation cross-sections computed in this work, (b) a constant cross-section of 2.5×10^{-19} cm^2, but with appropriate threshold photon energies for each $v''J''$ level as implemented in Shaw et al. (2005), and (c) neglect of direct continuum photodissociation. The constant value in model (b) was intended to approximate the vibrationally resolved cross sections obtained by Allison & Dalgarno (1969). All simulations include destruction of H_2 through the Solomon process, reaction (1), i.e., UV bound–bound excitation through the Lyman and Werner bands followed by fluorescence (or spontaneous radiative dissociation) into the $X^1\Sigma_g^+$ continuum. A total of nine simulations were performed with representative results given in Figures 6–9.

Figure 6 displays dissociation rates and the H_2 column density $N(H_2)$ for the Orion Veil (Model I). The Solomon process dominates for all cloud depths, whereas the rate computed for direct continuum dissociation is approximately a factor of two smaller. Furthermore, the rates computed from the current cross sections are more than an order of magnitude larger than those obtained in Model b. The total column density $N(H_2)$ is decreased somewhat over the entire range of A_V when the new direct photodissociation cross sections (Model a) are included compared to Model c. The constant cross-sections used in Model b give a similar result as found in Model c and is indistinguishable on the scale of the figure. The percentage change in the rovibrationally resolved column densities is given in Figure 7 as a function of v'' and J'' where it is seen that the largest effect ($\sim$10%) occurs for small J'' (< 4), but roughly independent of v''.

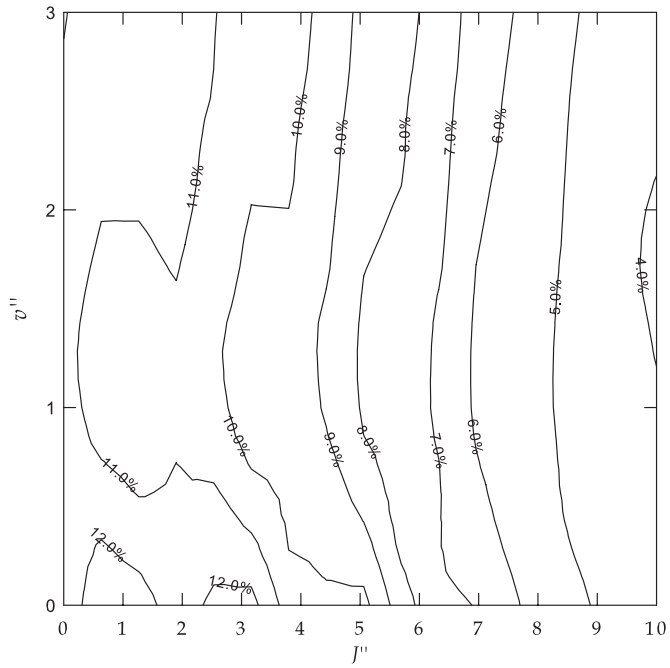

Figure 7. Percentage difference in column density $N(H_2)$ (v'', J) between using the H_2 direct photodissociation rate computed from this work (Model a) and neglecting direct photodissociation (Model c) for the Orion Veil (Model I) given as a function of v'' and J''.

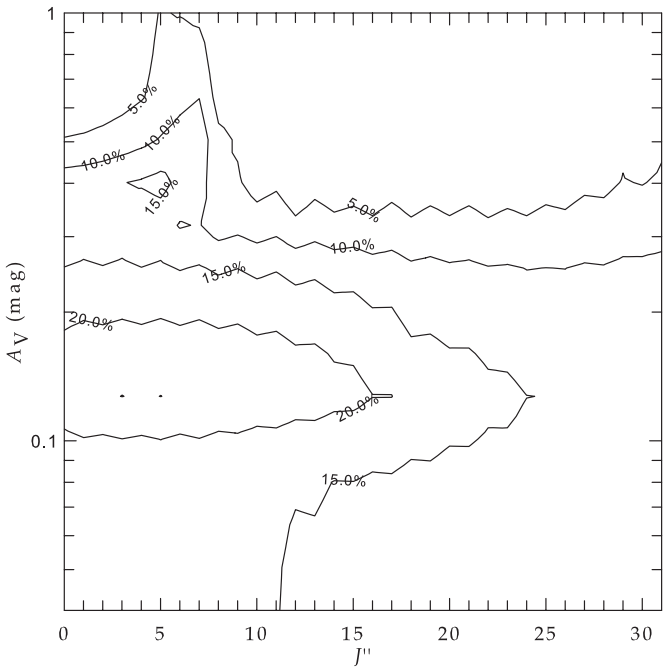

Figure 9. Percentage difference in column density $N(H_2)$ ($v'' = 0$, J'') between using the H_2 direct photodissociation rate computed from this work (Model a) and neglecting direct photodissociation (Model c) for the XDR (Model III) as a function of J'' and A_V.

Column densities $N(H_2)$ for the Leiden F2 model (Model II) were computed for all three photodissociation models (a–c), but the differences were found to be negligible suggesting that direct continuum photodissociation is unimportant in this case. This is not surprising as this model has practically no radiative flux beyond the Lyman limit.

Figure 8 compares for the XDR simulation (Model III), the photorates and H_2 column densities for cases (a), (b), and (c). The trends in the dissociation rates are very similar to those found for Model I, but with the direct dissociation rate being more comparable to the Solomon process to somewhat larger A_V. Figure 8 also demonstrates that direct photodissociation (Model a) reduces the total column density $N(H_2)$ over a broad region, but the reduction is not large. In Figure 9, we consider the effect on rotational column densities of H_2 due to direct continuum photodissociation for the XDR Model III.

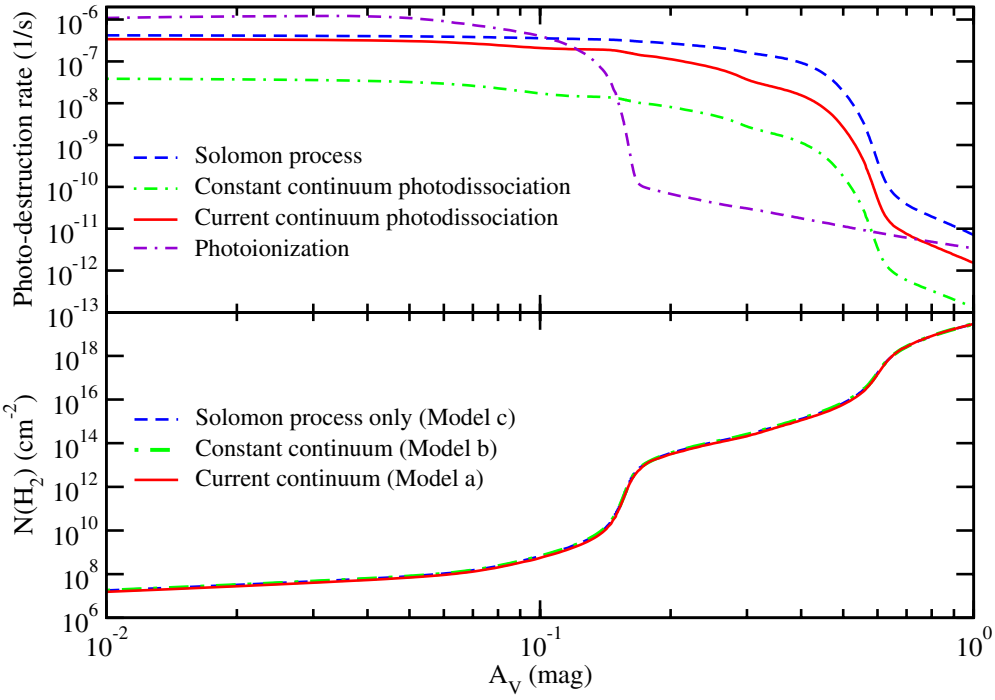

Figure 8. H_2 photodestruction rates (s^{-1}) and $N(H_2)$ (cm^{-2}) for the XDR model (Model III) as a function of visual extinction A_V.
(A color version of this figure is available in the online journal.)

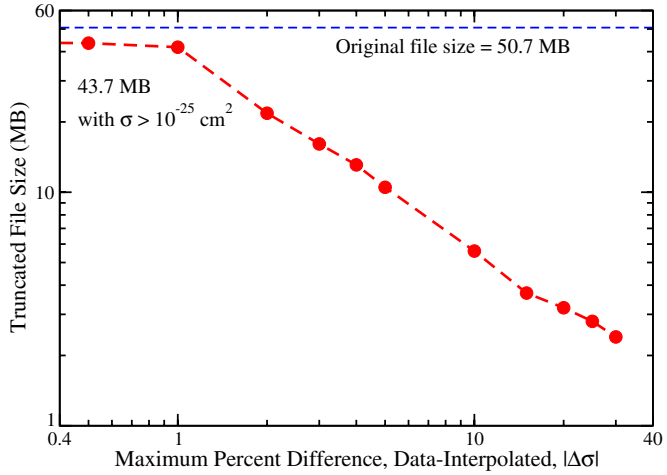

Figure 10. Continuum data file truncation. Truncated file size vs. the maximum percentage difference in allowed error of the interpolated data. $|\Delta\sigma|$ is defined as (data-interpolated)/data.

(A color version of this figure is available in the online journal.)

The percentage difference in column density between using the direct photodissociation rate computed from this work (Model a) and neglecting direct photodissociation (Model c) for $v'' = 0$ are shown as a function of A_V (very similar plots were obtained for $v'' = 1$ and 2, not shown). The largest effects occur for A_V between 0.1 and 0.2 and for $J'' < 15$ with the percentage change exceeding 20%.

While the focus of this work is v, J-resolved direct photodissociation, the photoionization rates of H_2 are also presented for Models I and III in Figures 6 and 8, respectively. In the Orion Veil case, the photoionization rate is seen to be smaller than both the Solomon and direct photodissociation rates, falling off rapidly for $A_V > 0.6$. However, the photoionization rate is obtained using only the $v'' = 0$, $J'' = 0$ cross-sections of Yan et al. (1998, 2001). In the XDR model, photoionization dominates the photodestruction of H_2 for $A_V < 0.1$ and $A_V > 2$. The inclusion of v, J-resolved photoionization rates is likely to enhance the destruction of H_2 in both models, particularly for A_V between 0.1 and 1.

Finally, UV-irradiated environments also contain significant photon fluxes in the H Lyman resonance lines which can contribute to photodestruction (note that this is implicitly included in the CLOUDY simulations). While the direct photodissociation cross sections for all H_2 rovibrational levels have thresholds with wavelengths less than Lyα, higher H Lyman lines may overlap with many rovibrationally excited cross-sections. Further, the photodissociation cross-sections typically display resonant features near threshold. If such resonant features are coincident with Lyβ, for example, the photodestruction rate may be enhanced. Three such coincidents were found: $v''J'' = (0, 22)$ and (2, 7) for the $B \leftarrow X$ transition and (0, 22) for $C \leftarrow X$. The former example is illustrated in Figure 5. However, while the $C^1\Pi$ electronic state is doubly degenerate, Λ-splitting in the continuum is not included in the photodissociation calculations. Therefore, the error in the location of the resonance can be estimated from the splitting of the rovibrational energies of the $C^1\Pi^+$ and $C^1\Pi^-$. For possible quasi-bound $v'J'$ levels, the splitting is $\lesssim$40 cm^{-1}, which is obtained from the highest-lying C rovibrational levels (Abgrall et al. 2000), but is comparable to the FWHM of both (0, 22) resonances.

3.3. Truncation of Continuum Cross-section Data Sets

As the photodissociation cross-sections computed here include 602 transitions obtained over a large wavelength range and calculated over a fine energy grid to resolve resonances, the file size of the resulting data set is relatively large. Since elaborate modeling packages strive to be comprehensive including a large range of species and processes and avoid the use of precomputed fits, the management of such data sets becomes problematic. We therefore explored a scheme to truncate data sets for continuum processes without loss of accuracy in the resulting models.

As most cross sections have a peak value of $\sim 10^{-18}$ cm^2, we arbitrarily removed computed points with cross-section values less than 10^{-25} cm^2. This reduced our file size from 50.7 MB to 43.7 MB. We then systematically removed data points whose cross-section differed by less than some value, $\delta\sigma$ (e.g., 10%), with a point adjacent in wavelength to create a truncated data file. We then interpolated the truncated data to compute the cross-section at each of the redacted points and calculated the percentage difference $\Delta\sigma$ with the original data. The algorithm was repeated on the original set varying $\delta\sigma$ until $\Delta\sigma$ was less than some specified value for all original data points. Figure 10 shows how the file size is decreased with increase in allowed $\Delta\sigma$. For example, choosing $\Delta\sigma = 30\%$ reduces the file size by a factor of 18. Linear interpolation of the truncated data reproduces all original data points to within a difference of 30%. The models computed here used a truncated data set with $\Delta\sigma = 10\%$.

While we provide all original data, the user could opt for such a truncation strategy choosing $\Delta\sigma$ to be consistent with the resolving power of relevant observational data or to speed up calculations when a large grid of models is to be performed. Some truncated data sets can be obtained from the UGAMOP Web site or Fortran routines for truncation can be obtained from the authors.

4. CONCLUSION

Rovibrationally resolved direct photodissociation cross-sections for H_2 have been computed for the Lyman and Werner transitions from all 301 $v''J''$ levels of the electronic ground state for photon wavelengths from 100 Å to threshold. The wavelength grid was chosen sufficiently small to resolve resonant features near threshold due to quasi-bound levels. The photodestruction rate due to direct photodissociation is demonstrated to be comparable to the dissociation rate due to fluorescent decay to the continuum following UV excitation through the Lyman/Werner bands (the so-called Solomon process) in simulations of a diffuse interstellar cloud and an XDR. Due to the sparseness of photons with energies beyond the Lyman limit, direct photodissociation of H_2 appears to play little role in typical PDRs. The H_2 rotational column densities are found to be affected by up to 20% in the XDR model when direct H_2 photodissociation is included. A prescription for reducing the file size of a continuum data set to within a given accuracy is provided.

We acknowledge support from NASA grant NNG06GJ11G from the Astrophysics Theory Program (C.D.G., P.C.S., G.J.F.) and program number HST-AR-11776.01-A (P.C.S., N.P.A.), which was provided by NASA through a grant from the Space Telescope Science Institute, which is operated by the Association of Universities for Research in Astronomy, Inc., under NASA contract NAS5-26555. P.A.M.v.H. acknowledges support from the Belgian Federal Science Policy Office via

the PRODEX Programme of ESA. We thank the referee for insightful comments.

REFERENCES

Abel, N. P., Brogan, C. L., Ferland, G. J., et al. 2004, ApJ, 609, 247
Abel, N. P., Dudley, C., Fischer, J., Satyapal, S., & van Hoof, P. A. M. 2009, ApJ, 701, 1147
Abel, N. P., Ferland, G. J., O'Dell, C. R., Shaw, G., & Troland, T. H. 2006, ApJ, 644, 344
Abel, N. P., Ferland, G. J., Shaw, G., & van Hoof, P. A. M. 2005, ApJ, 161, 65
Abgrall, H., Le Bourlot, J., Pineau des Forêts, G., et al. 1992, A&A, 253, 525
Abgrall, H., Roueff, E., & Drira, I. 2000, A&AS, 141, 297
Allison, A. C., & Dalgarno, A. 1969, At. Data, 1, 91
Bertoldi, F., & Draine, B. T. 1996, ApJ, 458, 222
Bukta, J. F., & Meath, W. J. 1974, Mol. Phys., 27, 1235
Cooley, J. W. 1961, Math. Comput., 15, 363
Coppola, C. M., Diomede, P., Longo, S., & Capitelli, M. 2011, ApJ, 727, 37
Draine, B. T. 2000, ApJ, 532, 273
Dressler, K., & Wolniewicz, L. 1985, J. Chem. Phys., 82, 10
Federman, S. R., Glassgold, A. E., & Kwan, J. 1979, ApJ, 227, 466
Ferland, G. J., Korista, K. T., Verner, D. A., et al. 1998, PASP, 110, 761
Haiman, Z., Rees, M. J., & Loeb, A. 1996, ApJ, 467, 522
Kirby, K. P., & van Dishoeck, E. F. 1988, Adv. At. Mol. Phys., 25, 437
Kolos, W., & Wolniewicz, L. 1965, J. Chem. Phys., 43, 7
Kolos, W., & Wolniewicz, L. 1968, J. Chem. Phys., 48, 3672
Meijerink, R., & Spaans, M. 2005, A&A, 436, 397
Miyake, S., Stancil, P. C., Sadeghpour, H. R., et al. 2010, ApJ, 709, L168
Röllig, M., Abel, N. P., Bell, T., et al. 2007, A&A, 467, 187
Shaw, G., Ferland, G. J., Abel, N. P., Stancil, P. C., & van Hoof, P. A. M. 2005, ApJ, 624, 794
Shull, J. M. 1978, ApJ, 219, 877
Stecher, T. P., & Williams, D. A. 1967, ApJ, 149, L29
Stephens, T. L., & Dalgarno, A. 1974, Mol. Phys., 28, 1049
Tiné, S., Lepp, S., Gredel, R., & Dalgarno, A. 1997, ApJ, 481, 282
van Hoof, P. A. M., Weingartner, J. C., Martin, P. G., Volk, K., & Ferland, G. J. 2004, MNRAS, 350, 1330
Weck, P. F., Stancil, P. C., & Kirby, K. 2003, ApJ, 582, 1263
Whiting, E. E., & Nicholls, R. W. 1974, ApJS, 27, 1
Wolniewicz, L. 1993, J. Chem. Phys., 99, 1851
Wolniewicz, L. 1995, J. Chem. Phys., 103, 1792
Yan, M., Sadeghpour, H. R., & Dalgarno, A. 1998, ApJ, 496, 1044
Yan, M., Sadeghpour, H. R., & Dalgarno, A. 2001, ApJ, 559, 1194
Yan, Z.-C., Babb, J. F., Dalgarno, A., & Drake, G. W. F. 1996, Phys. Rev. A, 54, 2824